



**HAL**  
open science

## Cellulose nanofibrils and silver nanowires active coatings for the development of antibacterial packaging surfaces

Hugo Spieser, Aurore Denneulin, Davide Deganello, David Gethin, Rajesh Koppolu, Julien Bras

### ► To cite this version:

Hugo Spieser, Aurore Denneulin, Davide Deganello, David Gethin, Rajesh Koppolu, et al.. Cellulose nanofibrils and silver nanowires active coatings for the development of antibacterial packaging surfaces. Carbohydrate Polymers, 2020, 240, pp.116305 -. 10.1016/j.carbpol.2020.116305 . hal-03490303

**HAL Id: hal-03490303**

**<https://hal.science/hal-03490303>**

Submitted on 22 Aug 2022

**HAL** is a multi-disciplinary open access archive for the deposit and dissemination of scientific research documents, whether they are published or not. The documents may come from teaching and research institutions in France or abroad, or from public or private research centers.

L'archive ouverte pluridisciplinaire **HAL**, est destinée au dépôt et à la diffusion de documents scientifiques de niveau recherche, publiés ou non, émanant des établissements d'enseignement et de recherche français ou étrangers, des laboratoires publics ou privés.



Distributed under a Creative Commons Attribution - NonCommercial 4.0 International License

# Cellulose nanofibrils and silver nanowires active coatings for the development of antibacterial packaging surfaces

Hugo Spieser<sup>a, b</sup>, Aurore Denneulin<sup>a</sup>, Davide Deganello<sup>b</sup>, David Gethin<sup>b</sup>, Rajesh Koppolu<sup>c</sup>, Julien Bras<sup>a, d</sup>

<sup>a</sup>*Univ. Grenoble Alpes, CNRS, Grenoble INP\*, LGP2, F-38000 Grenoble, France*

<sup>b</sup>*College of Engineering, Swansea University, Bay Campus, Crymlyn Burrows, Swansea SA1 8EN, UK*

<sup>c</sup>*Laboratory of Natural Materials Technology, Åbo Akademi University, 20500 Turku, Finland*

<sup>d</sup>*IUF, 75000 Paris, France*

Corresponding author:

aurore.denneulin@grenoble-inp.fr

+33(0)4 76 82 69 28

*Laboratory of Pulp and Paper Science and Graphic Arts*

*461, rue de la Papeterie*

*CS 10065*

*38402 Saint-Martin d'Hères – France*

**Abstract:** An active ink composed of cellulose nanofibrils and silver nanowires was deposited on flexible and transparent polymer films using the bar coating process, achieving controlled thicknesses ranging from 200 nm up to 2  $\mu$ m. For 350 nm thick coating on polyethylene terephthalate films, high transparency (75.6% transmittance) and strong reduction of bacterial growth equal to 89.3% and 100% was noted respectively against Gram-negative *Escherichia Coli* and Gram-positive *Staphylococcus Aureus* bacteria using AATCC contact active standard test. Retained antibacterial activity was found with films produced by reverse gravure roll-to-roll process, showing the promising capability of this antibacterial solution to be deployed industrially. Finally, the same ink was also deposited on polylactic acid substrate to investigate barrier properties: for 350 nm thick coating, a reduction of 49% of oxygen transmission rate (dry conditions) and 47% reduction of water vapor transmission rate was noted, proving the enhanced barrier properties of the coatings.

**Keywords:** cellulose nanofibrils, silver nanowires, transparent coatings, antibacterial activity, barrier properties, up-scaling

---

\* Institute of Engineering Univ. Grenoble Alpes

## 31 **1. Introduction**

32 In a high consumption society, production and global movement of food products is considerable  
33 and increasing continuously (Food and Agriculture Organization of the United Nations, 2019). **Food**  
34 **products are exposed to harsh conditions throughout all of the supply chain stages and packaging is today**  
35 **expected to meet more and more requirements.** Recent innovation has focused on the development of  
36 active packaging, which refers to the ability of a package to respond to an external stimulus (Yildirim et  
37 al., 2018). Within this framework, active packaging aims at increasing the shelf-life of a product by  
38 optimizing the condition inside the package, thus improving food quality and reducing food waste.

39 Antimicrobial food packaging has been studied extensively over the past 20 years and aspires to  
40 reduce pathogenic contamination **against bacteria, fungus or viruses (Sofi et al., 2018) with a preferred**  
41 **mode of action working by contact for consumer safety and environmental concern. (Kaur & Liu, 2016).**  
42 Silver nanoparticles (Ag NPs) have recently attracted a lot of attention since they display strong  
43 antibacterial activity and can help fighting against the increasing antibiotic resistance in pathogens (Rai et  
44 al., 2012). It has been established that the antibacterial effect of Ag NPs is attributed to the nanoscale of  
45 the particles itself along with the continuous release of silver ions (Morones et al., 2005). The morphology  
46 of Ag NPs plays a major role on their antimicrobial activity: the smaller the nanoparticle (the higher  
47 surface area) the more active they are against bacteria (Carlson et al., 2008). The shape of the nanoparticle  
48 is also important and the antibacterial activity decreases on progression from pyramids, cubes, spheres, to  
49 wire-like shape (Hong et al., 2016; Pal et al., 2007). **Different parameters also influence the antibacterial**  
50 **activity of Ag NPs such as surface charge, the presence of residual synthesis surfactants or capping agent,**  
51 **and Ag NPs crystallinity. (El Badawy et al., 2011; Kvítek et al., 2008; Smetana et al., 2008).**

52 One way to use Ag NPs in packaging applications is to incorporate them into a nanocomposite to limit  
53 nanoparticle migration. **Ag NPs have been recognized as potentially hazardous for health as studies have**  
54 **focused on evaluating their toxicity against in vivo and in vitro studies. There is still a lack of information**  
55 **and knowledge concerning the global health hazard on human, but Ag NPs are suggested to be mainly**  
56 **dangerous by oral and inhalation adsorption and silver accumulation in different organs leading to specific**  
57 **malfunctions (Korani et al., 2015). The potent activity of Ag NPs is dependent on a lot of factors such as**  
58 **size, surface chemistry, shape, etc. and more research is needed to have a full overview of the toxicity of**  
59 **Ag NPs toward the human body. It then appears obvious that the leaching of Ag NPs in antibacterial**  
60 **composite for food packaging application is an important parameter to address. Nanocellulose materials**  
61 **are biobased, biodegradable and biocompatible nanomaterials that are defined as cellulose particles with a**  
62 **nano-scale size for at least one of their dimensions. One of the established class of nanocellulose are**  
63 **cellulose nanofibrils (CNF) which come from the mechanical fibrillation of pulp suspension (Herrick et**

64 al., 1983; Turbak et al., 1983). CNF have been of particular interest because they display interesting  
65 properties for packaging applications: high oxygen barrier property, vast chemical functionalization  
66 possibilities and good mechanical properties. CNF can be used either alone as a free standing film or as a  
67 coating on classic plastic packaging or paper substrates for its reinforcement properties (Afra et al., 2016;  
68 Fukuzumi et al., 2009; Rodionova et al., 2012) and also display good matrix properties that can be used  
69 successfully to immobilize nanoparticles.

70 Combinations of Ag NPs and nanocellulose composites have been investigated extensively by the  
71 scientific community (Xu et al., 2017) and different composite preparation techniques exist. **In the most  
72 common in-situ synthesis methods, CNF serve as a template matrix for adsorption of silver salts, followed  
73 by in-situ chemical reduction (Uddin et al., 2017; Yu et al., 2019). Covalent bonding is another option ,yet  
74 to our knowledge**, the only reported example comes from Ramaraju, Imae, & Destaye (2015), who  
75 reported the immobilization of Ag NPs stabilized with a dendrimer by covalently bonding the NH<sub>2</sub>-  
76 terminated dendrimer on TEMPO-oxidized CNF. Finally, the physical mixing approach is just mixing  
77 separately produced components. **To our knowledge**, the only example of simple mixing of CNF materials  
78 with Ag NPs for antibacterial applications has been reported by Martins et al. (2012) who prepared  
79 CNF/Ag NPs composites based on a polyelectrostatic assembly for antibacterial coating on a paper  
80 substrate. **Simple mixing is a straightforward easily up-scalable procedure, however immobilization of the  
81 Ag NPs on cellulose materials is relatively poor (Ilić et al., 2009), leading to reduced life-time of the  
82 system and possible non-desired release of Ag NPs.**

83 This work presents the development of antibacterial packaging based on a combination of silver  
84 nanoparticles and nanocellulose materials. Indeed, based on the precedent literature review, it was then  
85 hypothesized that combining silver nanowires with cellulose nanofibrils could achieve easy-to-process  
86 systems that can be deposited on flexible substrate to achieve contact killing antibacterial mode of action  
87 along with improved barrier properties. In this study, the technical challenges were firstly to  
88 straightforwardly produce a transparent and antibacterial coating on plastic polymer sheets. Secondly the  
89 objectives were to prepare similar active coatings on biobased polymer sheets and to evaluate the  
90 enhancement of their barrier property. Finally, the challenge of preparing active surfaces with a roll-to-roll  
91 process for up-scaling purposes was addressed.

92 To tackle the three core challenges, a hybrid ink composed of TEMPO-oxidised cellulose nanofibrils and  
93 silver nanowires was firstly deposited on polyethylene terephthalate substrates using laboratory-scale bar  
94 coating process. **Thickness and transparency of the coatings were investigated and they were tested against  
95 bacterial contamination.** The same technique was used to deposit the active ink on bio-based polylactic  
96 acid sheets and the barrier properties of the produced films were characterized. Finally, a new lower cost

97 active ink was specifically formulated by the authors to assess the up-scaling possibility by using a reverse  
98 gravure roll-to-roll coating process.

## 99 **2. Materials and methods**

### 100 **2.1. Materials**

101 A polyethylene terephthalate (PET) sheet substrate (Melinex® ST726 – 175 µm) and polylactic acid  
102 (PLA) substrate (Earthfirst® BCWC – 75 µm) was respectively purchased from Dupont (France) and  
103 Sidaplast (Belgium). A hybrid ink system composed of silver nanowires (Ag NWs) and TEMPO oxidised-  
104 cellulose nanofibrils (T-CNF) in water (PolyBioWire® 9830C) was supplied by Poly-Ink (France) **with an**  
105 **approximate 1% wt total mass and 1:1 ratio given by the supplier. However to investigate a roll-to-roll**  
106 **semi-industrial deposition process, a new specific formulation was prepared, using T-CNF suspension**  
107 **(CNF-A13) from Betulium (Finland) with approximately length of 50-400 nm and diameter of 5-15 nm,**  
108 **at 5 %wt (charge density of  $1.6 \pm 0.1$  mmol.g<sup>-1</sup>, estimated aspect ratio of 22.5) and using 2.5% wt Ag NWs**  
109 **aqueous suspension (NGAP NF Ag-3170) from NanoGap (USA) with estimated length 10-50 µm,**  
110 **diameter 50-100 nm (and so with an estimated aspect ratio of 400).**

111 Escherichia Coli ATCC 8739 and Staphylococcus Aureus ATCC 6538 were purchased from  
112 Microbiologics (USA). PCA (Plate Counting Agar) was purchased from BD Difco (USA) and contains  
113 beef extract (3g.l<sup>-1</sup>), peptone (5g.l<sup>-1</sup>), agar (15g.l<sup>-1</sup>). Standard nutrient broth 1 was purchased from Roth  
114 (Germany) and contains beef extract (3g.l<sup>-1</sup>), peptone (15g.l<sup>-1</sup>), sodium chloride (6 g.l<sup>-1</sup>) and glucose (1g.l<sup>-1</sup>  
115 <sup>1</sup>). Sodium thiosulphate (>99%), L-histidine (>98.5%), potassium dihydrogen phosphate (>99%),  
116 Tween®80 and calcium chloride (>96%) were also obtained from Roth (Germany). L α-phosphatidyl  
117 choline (>99%) was purchased from Sigma Aldrich (France). All materials were used as received.

### 118 **2.2. Active layer production by bar coating process**

119 **Coated films were first prepared using the supplied T-CNF/Ag NWs ink and using the bar coating process**  
120 **(KCC101, Erichsen, Germany). Prior to coating, the films were corona treated (Klwar Calvatron SG2,**  
121 **Germany): 2 passes, 90° rotation between the pass. The coatings were then oven-dried and different**  
122 **thickness were achieved using different threaded rod diameter (Supplementary data). Coatings, corona**  
123 **treatment and drying step parameters were optimized through extensive research with visual observation**  
124 **of possible defects, transparency and sheet resistance measurements. Optimized corona treatment settings**  
125 **are the following: 2.9 m.min<sup>-1</sup> speed and 330 mA intensity for PET substrate, 3.5 m.min<sup>-1</sup> speed and 150**  
126 **mA intensity for PLA substrate. Optimized coatings and drying parameters are the following: coating**  
127 **speed of 5.4 m.min<sup>-1</sup> for both PET and PLA coatings, oven-drying step at 120°C for 60s for PET and at**

128 room temperature overnight for PLA coatings. Each coating was performed at least three times to assess  
129 consistency and reproducibility of the process.

### 130 **2.3. Structural and quality characterization**

131 Field-Emission Gun Scanning Electron Microscope (FEG-SEM) was used to investigate the hybrid  
132 nanostructure after 2 nm-coating of Gold /Palladium, at 5.4 mm working distance and 3 kV accelerating  
133 voltage. A cross-section through the coated samples was prepared using a LEICA UC6 (Germany)  
134 ultramicrotome apparatus equipped with a diamond knife, at room temperature and with a cutting speed of  
135 1 mm.s<sup>-1</sup>. The thickness of the coatings was then estimated by image analysis using FIJI software  
136 (Schindelin et al., 2012; Schneider et al., 2012). At least 6 measurements in three different positions in the  
137 films were considered.

138 Transmittance (%) was measured on a UV-spectrophotometer (Shimadzu Manufacturing Inc., USA),  
139 using the photometric mode. Six different measurements were conducted on each sample at 550 nm  
140 wavelength. Sheet resistance ( $\Omega$ /sq) of the coated layer was measured by a four-probe system (Jandel  
141 Universal, USA). The measurement was repeated at six positions on the film and the average computed  
142 along with associated standard deviation.

### 143 **2.4. Antibacterial characterization**

144 Prior to antibacterial testing, a leaching assay was performed by putting a 2 x 2 cm specimen of coating  
145 (24  $\mu$ m estimated wet thickness) in 10 ml of deionized water (DI), under agitation (100 rotation per  
146 minute) at 37°C. After 72 hours, the liquid media was recovered and full UV-vis spectra (300-700 nm  
147 wavelength, 1 nm scan rate) were recorded on a UV-spectrophotometer (Shimadzu Manufacturing Inc.,  
148 USA), and compared with Ag NWs suspensions at 0.005% wt.

149 All the glassware, consumables, tools and solutions used for the antibacterial characterization were  
150 sterilized prior to use in autoclave for 20min at 120°C and 1.034 bar.

151 Antibacterial activity was assessed initially using an inhibition zone qualitative test following a modified  
152 AFNOR EN 1104 standard (AFNOR standard, 2005). To exaggerate the antibacterial activity of the  
153 samples, the test was carried out on multilayer coating (10 layers) prepared with the same parameters as  
154 single layer coating (threaded rod with 1.27 diameter –100  $\mu$ m estimated wet thickness). Ag NWs only  
155 coating was used as control and prior to deposition, the starting suspension was diluted to 0.5% wt in DI  
156 and dispersed using an Ultra Turrax high shear disperser (30s, 10,000 rpm). The produced samples were  
157 cut into 5 cm x 5 cm specimens and dry-sterilized for 24 hours at 60°C. 10 ml of pre-inoculated PCA at

158  $10^5$  CFU.ml<sup>-1</sup> (Colony Forming Unit) was poured in a petri dish and after cooling the samples were put on  
159 top with the coated side facing the agar. The incubation period was 72 hours at 37°C and the inhibition  
160 zone was assessed visually after incubation.

161 Quantitative tests were performed on single layer coatings with different thickness using a protocol  
162 adapted from the AATCC TM100-1998 standard (AATCC standard, 1998). The samples were cut into 2  
163 cm x 2 cm specimens and dry-sterilized for 24 hours at 60°C. 200 µl of bacterial suspension at  $5.10^5$   
164 CFU.mL<sup>-1</sup> in 20% nutrient broth (5 g.l<sup>-1</sup> nutrient broth, 6.8 g.l<sup>-1</sup> sodium chloride) were deposited on the  
165 samples specimen and incubated at 37°C for 24 hours. After incubation, the bacterial suspension was  
166 recovered by washing with a prepared neutralizing solution (3 g.l<sup>-1</sup> of L- $\alpha$ -phosphatidyl choline, 5 g.l<sup>-1</sup> of  
167 sodium thiosulphate, 1 g.l<sup>-1</sup> of L-histidine, 30 g.l<sup>-1</sup> of Tween 80, 10 ml of potassium dihydrogen phosphate  
168 at 0.0425 g.l<sup>-1</sup>, controlled pH of  $7.2 \pm 0.2$ ) and the final concentration was determined by the plate  
169 counting numbering method. The antibacterial activity (AA, %) of the samples was compared  
170 quantitatively using the following equation (1):

$$171 \quad AA (\%) = \frac{BC_{reference} - BC_{sample}}{BC_{reference}} \times 100 \quad (1)$$

172 Where BC<sub>reference</sub> (log CFU) is the remaining bacterial concentration on the PET substrate with no coating  
173 and BC<sub>sample</sub> (log CFU) is the remaining concentration on the tested sample.

## 174 **2.5. Barrier properties characterization**

175 The Oxygen Transmission Rate (OTR) of the coated samples was measured at 0, 50 and 80 % humidity  
176 rate following the ASTM-F 1927-98 standards (ASTM standard, 2014) on a Systech Illinois Permeation  
177 Analyser (USA) equipped with a coulometric detector. **The tests were conducted at 23°C and with a 6.15**  
178 **cm<sup>-1</sup> exchange surface.** At least 3 different samples for each coating were tested and an average is  
179 computed along with the associated standard deviation.

180 Water Vapour Transmission Rate (WVTR) was also measured on the same samples following a slightly  
181 modified T 448 om-09 standard (TAPPI Standard, 2009). Around 30 g of anhydrous calcium dichloride  
182 salt was put in a metal cup covered by the test sample and closed by a rubber gasket and screw-down cap.  
183 The test was conducted at a regulated temperature (23°C) and humidity (50 %). The water-uptake of the  
184 anhydrous salt through the tested sample was monitored by weighing at least twice a day for at least one  
185 week. The WVTR value was calculated using the following equation (2):

$$186 \quad WVTR (g.m^{-2}.day^{-1}) = \frac{24 \times \Delta m}{\Delta t \times S} \quad (2)$$

187 Where  $\Delta t$  (h) is the time between two measurements,  $\Delta m$  (g) the corresponding weigh-uptake and  $S$  ( $m^2$ )  
188 is the exposed surface ( $6.15 \text{ cm}^2$ ).

## 189 **2.6. Specific ink formulation and characterization for up-scaling test**

190 A specific, lower cost and in bigger volume formulation was prepared using T-CNF suspension  
191 (Betulium) and Ag NWs suspension (NanoGap) redispersed together at 1% wt total mass with a mass ratio  
192 of 1:1 using an Ultra Turrax high shear disperser (30s, 10,000 rpm).

193 T-CNF was imaged using a Philips CM 200/FEI (USA) Transmission Electron Microscope (TEM)  
194 equipped with a TemCam F216 from TVIPS (Germany), at 200 kV acceleration voltage. A diluted  
195 suspension of T-CNF was drop-casted on a copper grid with an amorphous carbon coating and uranyl  
196 acetate (2%) dye was deposited on the drop-casted sample. AFM images were recorded on a Veeco  
197 NanoScope-V apparatus (Canada). Ag NWs suspension was drop-casted on a Mica substrate and dried  
198 overnight. A tapping mode with an OTESPA Bruker (USA) silicon cantilever was used covering a  $3.3 \mu\text{m}$   
199  $\times 3.3 \mu\text{m}$  surface area.

200 The sedimentation evolution of the formulated ink was characterized by putting 10 ml of ink into a  
201 cylindrical glass vial of 29 mm diameter section and measuring the sediment height after a fixed time. The  
202 sediment height ( $S$ , %) was calculated using the following equation (3):

$$203 \quad S = \frac{H}{H_0} \times 100 \quad (3)$$

204 Where  $H$  (mm) is the measured sediment height and  $H_0$  (mm) the total liquid height.

205 The rheological studies were performed on a rotational rheometer (MCR02, Anton Paar) at a set  
206 temperature of  $20^\circ\text{C}$  with a cone-plate geometry ( $1.013^\circ$  angle, 50 mm diameter and  $55 \mu\text{m}$  truncate)  
207 along with a set gap of 0.112 mm. Flow curves experiment were performed with increasing shear rate  
208 ranging from 0.1 to  $1000 \text{ s}^{-1}$ .

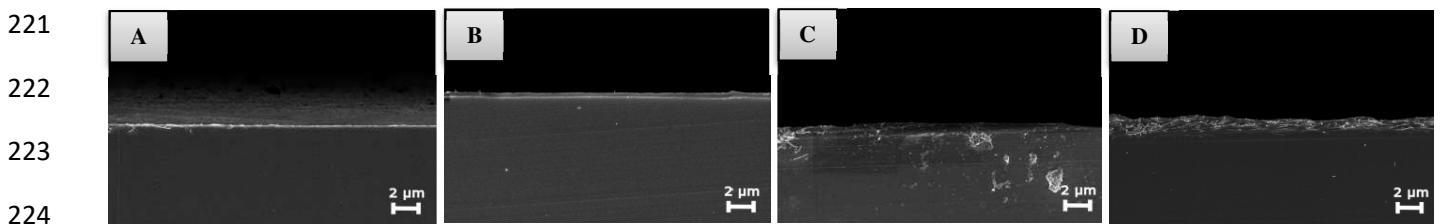
209 Reverse gravure coating was conducted using a Mini-Labo<sup>TM</sup> apparatus from MIRWEC Film, Inc./ Yasui  
210 Seiki company (USA). Coating was applied at a speed of  $1 \text{ m}\cdot\text{min}^{-1}$  and dried using infrared heaters. Two  
211 different coating weights were produced using two different gravure rolls: roll 30 (estimated surface  
212 volume of  $150 \text{ cm}^3\cdot\text{m}^{-2}$ , estimated transfer fraction of 0.33 and estimated approximate wet coat thickness  
213 of  $30\text{-}45 \mu\text{m}$ ), and roll 120 (estimated surface volume of  $34.7 \text{ cm}^3\cdot\text{m}^{-2}$ , estimated transfer fraction of 0.28  
214 and estimated approximate wet coat thickness of  $5\text{-}11 \mu\text{m}$ ).



215 **3. Results and discussion**

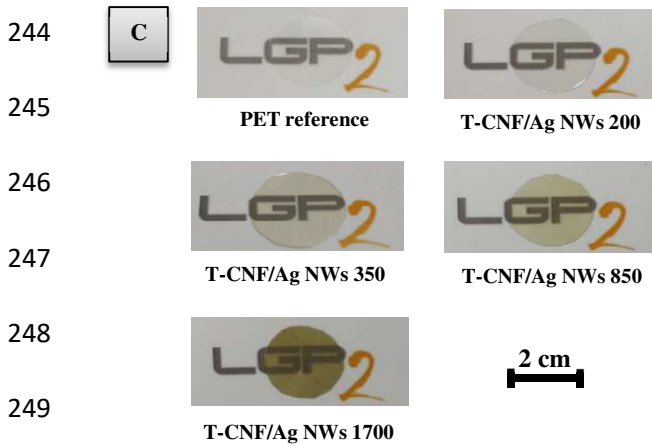
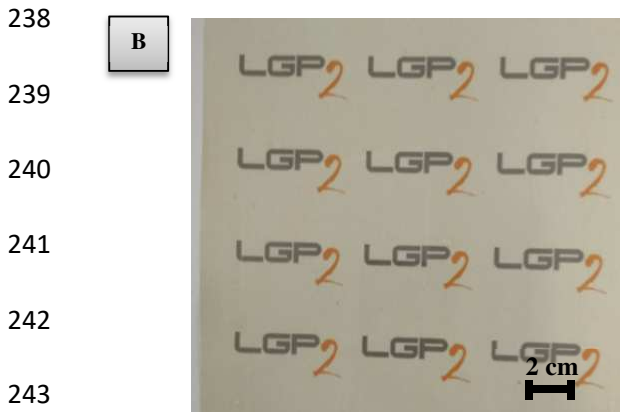
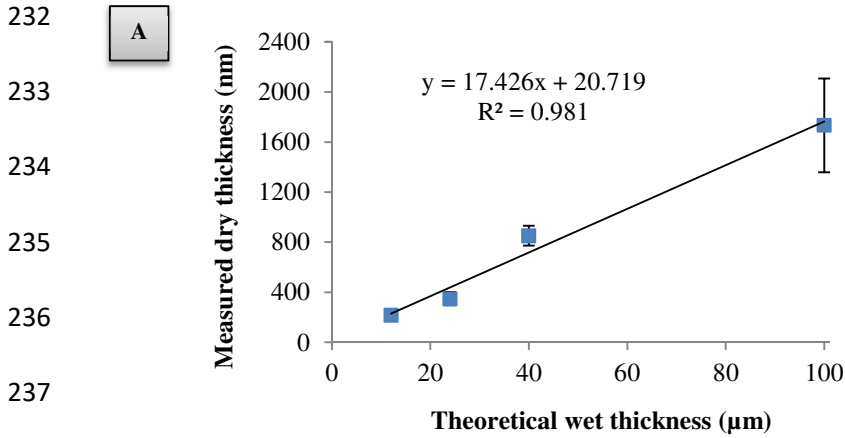
216 **3.1. Bar coating deposition on PET and antibacterial properties.**

217 The active ink was bar coated at 4 different thicknesses on PET sheets and the dry thickness was  
218 determined from a cross section captured by FEG-SEM imaging (Figure 1). For the thicker coatings the  
219 results demonstrated a higher standard deviation because the ultramicrotome cuts damaged the coated  
220 layer.



225 **Figure 1: FEG-SEM cross section images of A) 12 μm wet estimated thickness coating B) 24 μm wet**  
226 **estimated thickness coating C) 40 μm wet estimated thickness coating D) 100 μm wet estimate thickness**  
227 **coating**

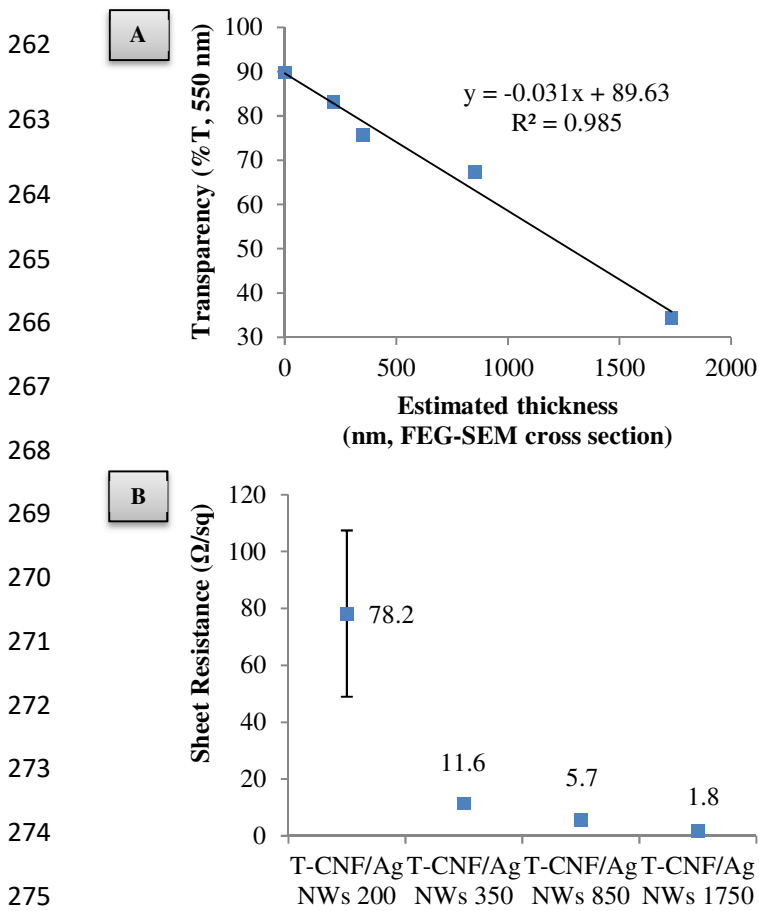
227 The measured average thicknesses are respectively  $217 \pm 27$ ,  $349 \pm 52$ ,  $851 \pm 79$  and  $1733 \pm 375$  nm. A  
228 good linear correlation was found between wet and dry values (Figure 2A) proving a controlled thickness  
229 deposition and accurate measurement. Consequently, in this study the samples will be designated T-  
230 CNF/Ag NWs 200, T-CNF/Ag NWs 350, T-CNF/Ag NWs 850, T-CNF/Ag NWs 1750, referred according  
231 to their dry thickness.



250 **Figure 2: Coating quality investigated by A) measured**  
 251 **dried thickness (nm) vs theoretical wet thickness (µm), B)**  
 252 **qualitative picture of 15 cm x 15 cm large area of T-**  
 253 **CNF/Ag NWs 350 sample and B) qualitative picture of**  
 254 **reduced area of all produced samples (2 cm diameter) and**  
 255 **scale bar.**

253 From a macroscopic point of view, the coatings were observed to be uniform with no local uncoated  
 254 patches (Figure 2B). For packaging applications, one of the key parameters for active coatings is to retain

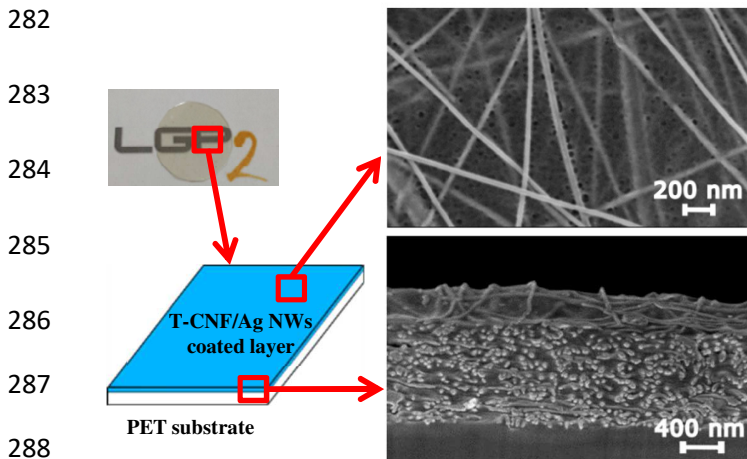
255 transparency for the purpose of aesthetics and product display. The coatings were found to be relatively  
 256 transparent as the LGP2 logo is clearly visible under the different samples displayed in Figure 2C. The  
 257 transmittance at 550 nm was measured at 83.3, 75.6 and 67.3% respectively for T-CNF/Ag NWs 200, T-  
 258 CNF/Ag NWs 350 and T-CNF/Ag NWs 850 samples, when compared to the 89.8% reference uncoated  
 259 PET. Coating quality may also be determined by measuring conductivity (Fahad et al., 2019) and except  
 260 for T-CNF/Ag NWs 200, the produced coatings display high conductivity (low sheet resistance) with a  
 261 very low standard deviation, confirming coating uniformity (Figure 3B).



276 **Figure 3: Coatings quality assessment using A)**  
 277 **transparency measurement (% T, 550 nm) vs**  
 278 **estimated dry thickness (nm) and B) sheet resistance**  
 279 **measurements by 4-probe system (Ω /sq).**

278 The morphology of the coated layer was also investigated using electron microscopy imaging (Figure 4)  
 279 and the coated layer was found to be highly organized in a dense network, yet not aggregated, with an  
 280 orientation of the Ag NWs toward the direction of shearing during the bar coating process.

281

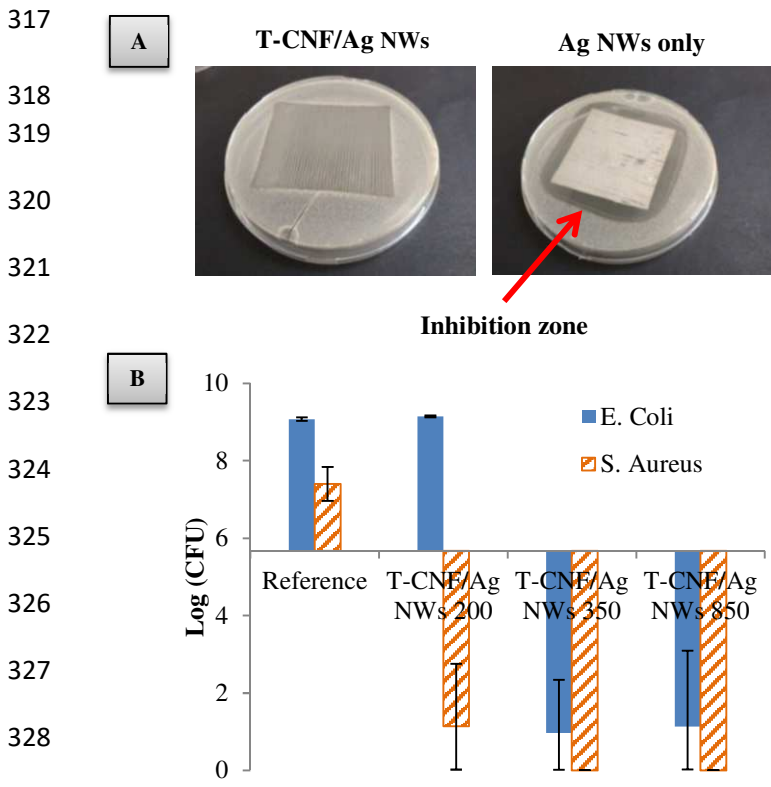


289 **Figure 4: Schematic view of the T-CNF/Ag NWs 850**  
 290 **coated samples and FEG-SEM pictures of surface and**  
 291 **cross-section**

291 A preliminary leaching study was performed prior to antibacterial characterization. The test showed that  
 292 no peaks corresponding to Ag NWs could be seen after recording UV-vis spectra of the recovered liquid  
 293 media after the leaching assay (Supporting Information). It can then be concluded that there is only limited  
 294 leaching of Ag NWs measured by this technique. The antibacterial activity of the active coatings was then  
 295 investigated with qualitative inhibition zone test (Figure 5A). For the sample coated only with Ag NWs, a  
 296 broad inhibition zone is visible proving the antibacterial activity of Ag NWs. The antibacterial activity of  
 297 Ag NWs was established to be mainly due to the release of silver ions because of their lower surface area  
 298 and thus lower adhesion with bacteria cell walls compared to spherical or cubic silver nanoparticles (Hong  
 299 et al., 2016; Visnapuu et al., 2013). It can then be assumed that the broad inhibition zone of the sample is  
 300 due to the release of silver ions into the media. For the sample coated with the mixture of both T-CNF and  
 301 Ag NWs no inhibition zone can be seen which suggests that physically entrapping the Ag NWs within the  
 302 T-CNF matrix leads to a contact killing mode of action with no or minimal release of active material.

303 To quantitatively verify the activity of the sample the AATCC standard method was performed against  
 304 both Gram-positive *Staphylococcus Aureus* and Gram-negative *Escherichia Coli* (Figure 5B). The T-  
 305 CNF/Ag NWs 200 sample show a surprising activity: it displays no impact against *E. Coli* whereas for *S.*  
 306 *Aureus*, a strong reduction of 6.3 log of colony forming unit compared to the uncoated reference sample  
 307 was noted, which corresponds to a 86.5% activity. Indeed, the bacterial activity in the presence of silver  
 308 nanoparticles is usually higher for *E. Coli* than *S. Aureus* (Chernousova & Epple, 2013). This is explained  
 309 by the difference in the bacteria cell wall: Gram-positive bacteria display a more permeable layer made of  
 310 peptidoglycan only whereas Gram-negative bacteria have a thinner yet more impermeable  
 311 lipopolysaccharide layer coupled to a thin peptidoglycan layer (Slavin et al., 2017). The difference in

312 activity observed when compared with the literature could be explained by the very thin coating layer for  
 313 T-CNF/Ag NWs 200 which is probably close to the antibacterial activity limit of the coating. The T-  
 314 CNF/Ag NWs 350 and T-CNF/Ag NWs 850 coatings displayed more or less the same performance  
 315 respectively 89.3% vs *E. Coli*/100% vs *S. Aureus* and 87.6% vs *E. Coli*/100% vs *S. Aureus*, showing that a  
 316 350 nm thick coating is enough to achieve almost 100% antibacterial activity.

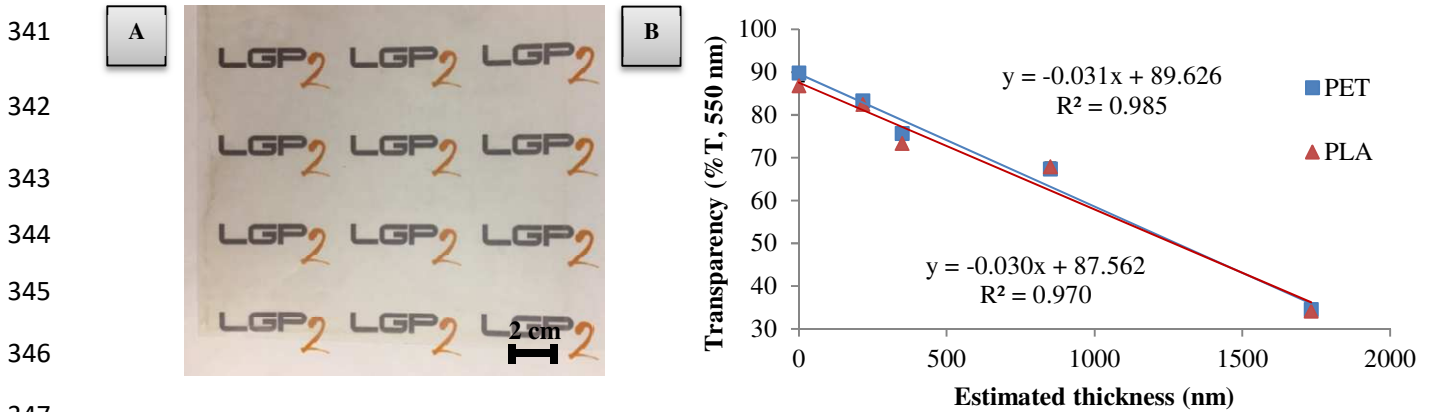


330 **Figure 5: Antibacterial characterization of the coated samples by A) inhibition qualitative analysis for *E. Coli* bacteria strain B) qualitative analysis using AATCC standard method 100-1998 vs *E. Coli* and *S. Aureus* with results expressed in log of colony forming units (log CFU).**

333 **3.2. Bar coating on PLA and barrier properties.**

334 In order to explore a bio-based substrate, the same ink was also deposited on polylactic acid (PLA) films  
 335 using the bar coating process. **The coatings were found to be homogeneous, with no uncoated patches and**  
 336 **no visual defects (Figure 6A).** The different deposited thickness for the PLA coatings were estimated to be  
 337 relatively close to the ones for the PET coatings. Indeed, the decrease of the transparency of the reference  
 338 films due to the coating are more or less the same for both the PET and PLA coatings (Figure 6B). The

339 samples were then named with the same code, for instance T-CNF/Ag NWs 350 PLA corresponds to the  
340 T-CNF/Ag NWs coating on PLA with an approximated thickness of 350 nm.



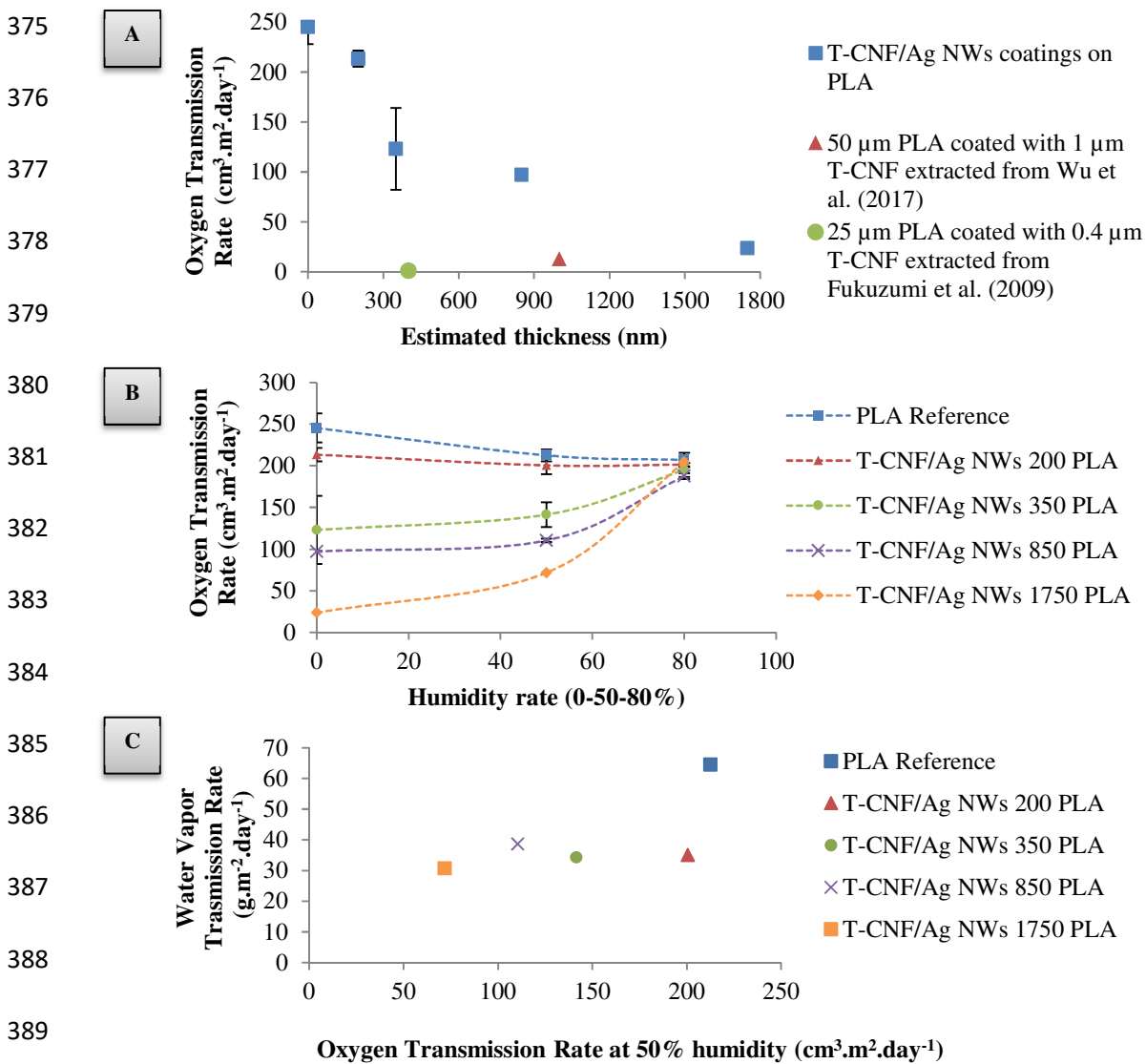
347 **Figure 6: T-CNF/Ag NWs coating on PLA quality assessment with A) picture of 15 cm x 15 cm large area of**  
348 **T-CNF/Ag NWs 350 sample and B) transparency (% T, 550nm) measurements and comparison with coatings**  
**on PET.**

349 **CNF are often used in packaging application for their interesting barrier properties (Ferrer et al., 2017)**  
350 **and so the barrier properties of the coated PLA was investigated.** Under dry conditions, the oxygen  
351 transmission rate (OTR) of the produced films was significantly decreased achieving more than 90%  
352 reduction for an estimated 1750 nm thick coatings (Figure 7A) but the measured values are however  
353 higher than those classically found in the literature for a T-CNF coating (Fukuzumi et al., 2009; Wu et al.,  
354 2017) (Figure 7A). Surprisingly in this study coating only T-CNF material was not possible due to high  
355 **dewetting** and so it was not possible to compare T-CNF/Ag NWs coatings to T-CNF coating only. A  
356 stronger surface treatment may be required to achieve T-CNF only coatings. **CNF performance as a barrier**  
357 **layer is generally explained first by the large specific surface area and dense network of hydrogen bonding**  
358 **of the material which makes it difficult for any molecules to pass through (Ferrer et al., 2017). The CNF**  
359 **network also presents high tortuosity due to the impermeable crystalline regions and strong entanglement**  
360 **of the flexible fibres presenting a capability to seal any gaps within the network (Lagaron et al., 2004;**  
361 **Syverud & Stenius, 2008; Belbekhouche et al., 2011).** Adding larger and rigid Ag NWs into the T-CNF  
362 matrix probably led to a physical disruption of the sealed network and thus explaining the difference  
363 between the measured properties and the ones described in the literature.

364 As expected from using CNF materials, the OTR measurement is humidity dependent (Figure 7B) and at  
365 high humidity (80%) the OTR values of the different coatings are close to the uncoated PLA reference.  
366 **The different coatings also showed a significant improvement of the WVTR values (Figure 7C) which is**  
367 **relatively similar (around 50% reduction) for all of the samples. This is interesting as coating CNF on**  
368 **polymer substrate usually leads to unchanged or slightly reduced water vapor permeability (Aulin et al.,**

369 2013; Vartiainen et al., 2017), due to the hydrophilic nature and low water resistance of such materials.  
 370 (Nair et al., 2014).

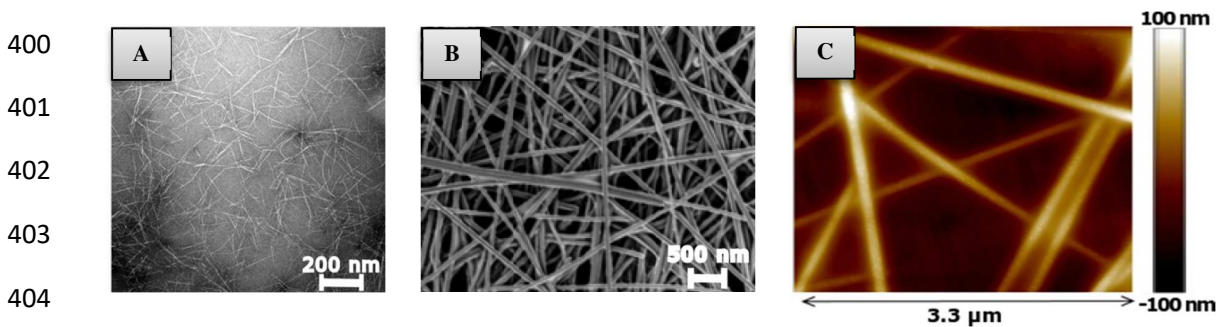
371 Coatings on biopolymer PLA sheets were successfully conducted and the coatings were found to be  
 372 homogeneous with no uncoated patches and no visual defects. The deposited layers were found to be  
 373 relatively similar to the coatings on PET and significant decrease for both the oxygen transmission rate  
 374 and water vapour transmission rate was noted, proving the enhanced barrier properties.



390 **Figure 7: PLA coatings barrier properties characterizations with A) Oxygen Transmission Rate**  
 391 **( $\text{cm}^3 \cdot \text{m}^{-2} \cdot \text{day}^{-1}$ ) measurements in dry conditions vs estimated coating thickness (nm) and**  
 392 **comparison with literature data B) Oxygen Transmission Rate ( $\text{cm}^3 \cdot \text{m}^{-2} \cdot \text{day}^{-1}$ ) measurements at**  
 393 **different humidity rate (0-50-80%) and C) Water Vapor Transmission Rate ( $\text{g} \cdot \text{m}^{-2} \cdot \text{day}^{-1}$ ) vs**  
 394 **Oxygen Transmission Rate ( $\text{cm}^3 \cdot \text{m}^{-2} \cdot \text{day}^{-1}$ ) at 50% of humidity.**

393 **3.3. Up-scaling**

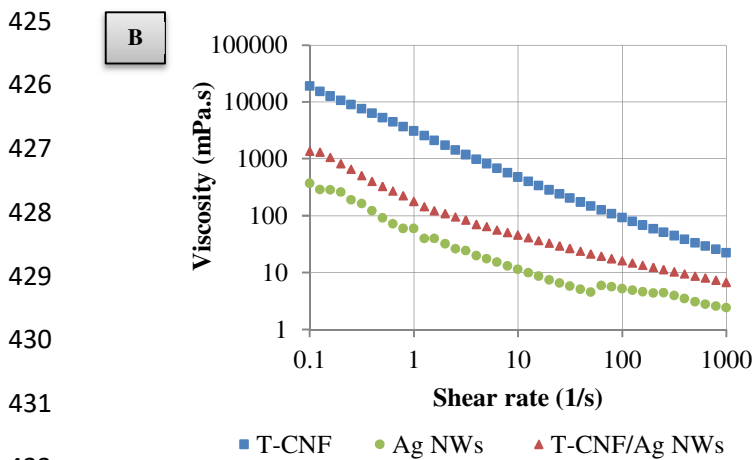
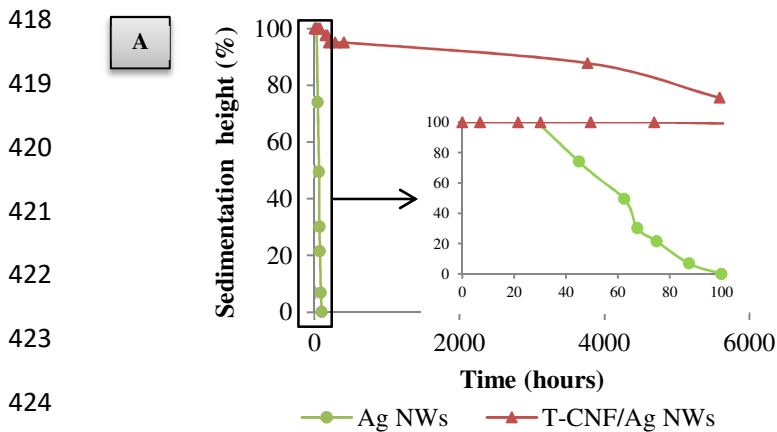
394 As a more direct route and from a more economical point of view, a similar antibacterial ink was  
395 specifically formulated by simple mixing and redispersion of the separately supplied components T-CNF  
396 and Ag NWs in deionized water (see Materials and methods). The purchased T-CNF possess small  
397 dimensions (approximately length 50-400 nm, diameter: 5-15 nm) and are rather rigid, as shown in the  
398 TEM images in Figure 8A. The silver nanowires dimensions were approximately one order of magnitude  
399 higher than the T-CNF: estimated length 10-50  $\mu\text{m}$ , diameter 50-100 nm (Figure 8B and C).



405 **Figure 8: Raw materials microscopy imaging for A) TEM images of T-CNF B) SEM**  
406 **images of silver nanowires C) AFM images of silver nanowires**

406 As it has already been described elsewhere (Hoeng et al., 2016), the T-CNF/Ag NWs ink is relatively  
407 stable over time and exhibits a very low sedimentation rate, for example 75% sedimentation height after 8  
408 months of testing, as compared to the Ag NWs suspension without T-CNF, that sedimented completely  
409 after 4 days (Figure 9A). Flow curve rheology experiments were performed to assess the possibility to use  
410 coating process for ink deposition and both materials and the final formulation display classic strong shear  
411 thinning behaviour (Herrick et al., 1983; Hoeng et al., 2017) (Figure 9B). These behaviours can be  
412 explained by the high aspect ratio of the nanoparticles in these colloidal suspensions and the induced  
413 alignment of the particles at high shear rate, thus decreasing the viscosity. Ink viscosity at high shear rate  
414 was found to be in line with was expected for the bar coating process. It was found that for the different  
415 tested shear rate, viscosity of T-CNF suspension was one order of magnitude higher than Ag NWs. T-CNF  
416 dictates the viscosity in the T-CNF/Ag NWs ink by acting as a rheological modifier which was already  
417 shown in the literature for other aqueous CNF suspension coatings (Grüneberger et al., 2014).





433 **Figure 9: Ink formulation characterization compared to raw materials with A) sedimentation height measurement (%) and B) rheological flow curves. All formulations are at 1% wt total concentration.**

435 **3.3. Roll-to-roll process deposition**

436 The potential for this formulation to be applied to industrial-like roll-to-roll coating process was also

437 investigated using a reverse gravure coating process. **Reverse gravure coating is interesting for packaging**

438 **applications because of the wide range of inks and substrate that can be used and was also chosen because**

439 **of the versatility of the process and the possibility to deposit low coat weights with a uniform and**

440 **controlled thickness (Kipphan, 2001; Vak et al., 2016).** Two different coating thicknesses were

441 investigated and designated after their estimated wet thickness and previously established wet

442 thickness/dry thickness relation for the bar-coated samples. In other words, T-CNF/Ag NWs 850RR for

443 the coating using the roll 30 (wet coat thickness of 30-45  $\mu\text{m}$ ), and T-CNF/Ag NWs 200RR for the

444 coating using roll 120 (wet coat thickness of 5-11  $\mu\text{m}$ ). **The coatings were found to be visually of high**

445 **quality with no uncoated patches, no visual defects and good homogeneity (Figure 10A).** The antibacterial

446 properties of the T-CNF/Ag NWs 200RR is relatively low whereas T-CNF/Ag NWs 850RR display a

447 strong antimicrobial effect (Figure 10B). The T-CNF/Ag NWs 850RR sample showed a strong and  
448 significant bactericidal effect, precisely 7.22 log reduction corresponding to 77.9% calculated antibacterial  
449 activity against *E. Coli* and 100% against *S. Aureus*. On the other hand, the T-CNF/Ag NWs 200RR  
450 sample showed no activity at all against *S. Aureus* whereas it showed a 7.57 log reduction corresponding  
451 to 81.7% activity against *E. Coli*. The measured antibacterial activity for the roll-to-roll coated samples  
452 using the up-scaled ink formulation were found to be in line with the results for the bar coated samples  
453 and thus the proposed solution for antibacterial packaging could hence be easily adapted to an industrial  
454 scale.

455

456

457

458

459

460

461



462

463

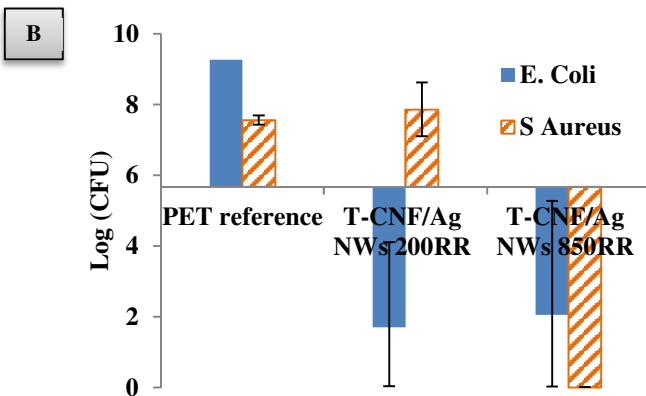
464

465

466

467

468



469

**Figure 10: Roll-to-roll coatings with A) visual aspect of the coatings and B) AATCC qualitative method for antibacterial activity assessment.**

#### 470 **4. Conclusion**

471 This work demonstrated the antibacterial activity of a hybrid system composed of TEMPO-oxidised  
472 cellulose nanofibrils and silver nanowires, coated as thin layers on different flexible polymeric substrate.  
473 The controlled thickness of the coatings on PET ranged from 200 to 1750 nm with a high relative  
474 transparency superior to 65%. The antibacterial activity was suggested to work by contact active killing  
475 mode of action and for the 350 nm thick coating, a significant AATCC standard antibacterial activity of  
476 89.3% and 100% was noted respectively against Gram-negative *Escherichia Coli* and Gram-positive  
477 *Staphylococcus Aureus* bacteria. Moreover, the same ink was also deposited on PLA sheets with similar  
478 estimated thickness and quality. After coating, oxygen and water vapour permeability of the PLA  
479 substrate was significantly reduced, respectively 49% of oxygen transmission rate (dry conditions) and  
480 47% reduction of water vapor transmission rate for 350 nm thick coating. Finally, a similar ink with lower  
481 cost materials was specifically formulated for up-scaling purposes and producing active surfaces using a  
482 roll-to-roll process was proved using the reverse gravure process, showing a strong retained antibacterial  
483 activity. Perspectives for a future work would be investigation of the migration of silver ions within the  
484 cellulose nanofibrils matrix and the influence of matrix surface chemistry.

485 **Declaration of competing interest**

486 The authors declare that there is no conflict of interests with this manuscript.

487 **Acknowledgements**

488 This research was supported LabEx Tec 21 (Grant agreement No. ANR-11-LABX-0030). This research  
489 was made possible thanks to the facilities of the TekLiCell platform funded by the Région Rhône-Alpes  
490 (ERDF: European regional development fund). Authors want to thank Bertine Khelifi from Grenoble INP  
491 Pagora for the SEM-FEG imaging and Christine Lancelon-Pin from Cermav for the ultramicrotome cross-  
492 section preparation.

493 **References**

- 494 AATCC standard. (1998). *TM100 - Test Method for Antibacterial Finishes on Textile Materials:*  
495 *Assessment of Antibacterial Textile*. AATCC, Research Triangle Park, NC.
- 496 AFNOR standard. (2005). *NF EN 1104 - Papier et carton destinés à entrer en contact avec les denrées*  
497 *alimentaires : Détermination du transfert des constituants antimicrobiens*. AFNOR Association,  
498 La Plaine Saint-Denis, France.
- 499 Afra, E., Mohammadnejad, S., & Saraeyan, A. (2016). Cellulose nanofibils as coating material and its  
500 effects on paper properties. *Progress in Organic Coatings*, *101*, 455–460.  
501 <https://doi.org/10.1016/J.PORGCOAT.2016.09.018>
- 502 ASTM standard. (2014). *F1927, 14 - Test Method for Determination of Oxygen Gas Transmission Rate,*  
503 *Permeability and Permeance at Controlled Relative Humidity Through Barrier Materials Using a*  
504 *Coulometric Detector*. ASTM International, West Conshohocken PA.
- 505 Aulin, C., Karabulut, E., Tran, A., Wågberg, L., & Lindström, T. (2013). Transparent Nanocellulosic  
506 Multilayer Thin Films on Polylactic Acid with Tunable Gas Barrier Properties. *ACS Applied*  
507 *Materials & Interfaces*, *5*(15), 7352–7359. <https://doi.org/10.1021/am401700n>
- 508 Belbekhouche, S., Bras, J., Siqueira, G., Chappey, C., Lebrun, L., Khelifi, B., Marais, S., & Dufresne, A.  
509 (2011). Water sorption behavior and gas barrier properties of cellulose whiskers and microfibrils  
510 films. *Carbohydrate Polymers*, *83*(4), 1740–1748. <https://doi.org/10.1016/j.carbpol.2010.10.036>
- 511 Carlson, C., Hussain, S. M., Schrand, A. M., Braydich-Stolle, L. K., Hess, K. L., Jones, R. L., & Schlager,  
512 J. J. (2008). Unique cellular interaction of silver nanoparticles: size-dependent generation of  
513 reactive oxygen species. *The Journal of Physical Chemistry. B*, *112*(43), 13608–13619.  
514 <https://doi.org/10.1021/jp712087m>
- 515 Chernousova, S., & Epple, M. (2013). Silver as Antibacterial Agent: Ion, Nanoparticle, and Metal.  
516 *Angewandte Chemie International Edition*, *52*(6), 1636–1653.  
517 <https://doi.org/10.1002/anie.201205923>
- 518 El Badawy, A. M., Silva, R. G., Morris, B., Scheckel, K. G., Suidan, M. T., & Tolaymat, T. M. (2011).  
519 Surface Charge-Dependent Toxicity of Silver Nanoparticles. *Environmental Science &*  
520 *Technology*, *45*(1), 283–287. <https://doi.org/10.1021/es1034188>
- 521 Fahad, S., Yu, H., Wang, L., Zain-ul-Abdin, Haroon, M., Ullah, R. S., Nazir, A., Naveed, K.-R.,  
522 Elshaarani, T., & Khan, A. (2019). Recent progress in the synthesis of silver nanowires and their  
523 role as conducting materials. *Journal of Materials Science*, *54*(2), 997–1035.  
524 <https://doi.org/10.1007/s10853-018-2994-9>
- 525 Ferrer, A., Pal, L., & Hubbe, M. (2017). Nanocellulose in packaging: Advances in barrier layer  
526 technologies. *Industrial Crops and Products*, *95*(Supplement C), 574–582.  
527 <https://doi.org/10.1016/j.indcrop.2016.11.012>
- 528 Food and Agriculture Organization of the United Nations. (2019). *World food and agriculture: statistical*  
529 *pocketbook 2019*.
- 530 Fukuzumi, H., Saito, T., Iwata, T., Kumamoto, Y., & Isogai, A. (2009). Transparent and High Gas Barrier  
531 Films of Cellulose Nanofibers Prepared by TEMPO-Mediated Oxidation. *Biomacromolecules*,  
532 *10*(1), 162–165. <https://doi.org/10.1021/bm801065u>
- 533 Grüneberger, F., Künniger, T., Zimmermann, T., & Arnold, M. (2014). Rheology of nanofibrillated  
534 cellulose/acrylate systems for coating applications. *Cellulose*, *21*(3), 1313–1326.  
535 <https://doi.org/10.1007/s10570-014-0248-9>

- 536 Herrick, F. W., Casebier, R. L., Hamilton, J. K., & Sandberg, K. R. (1983). Microfibrillated Cellulose:  
537 Morphology and Accessibility. *J. Appl. Polym. Sci.: Appl. Polym. Symp.*; (United States), 37.  
538 <https://www.osti.gov/scitech/biblio/5039044>
- 539 Hoeng, F., Denneulin, A., Krosnicki, G., & Bras, J. (2016). Positive impact of cellulose nanofibrils on  
540 silver nanowire coatings for transparent conductive films. *Journal of Materials Chemistry C*,  
541 4(46), 10945–10954. <https://doi.org/10.1039/C6TC03629E>
- 542 Hoeng, F., Denneulin, A., Reverdy-Bruas, N., Krosnicki, G., & Bras, J. (2017). Rheology of cellulose  
543 nanofibrils/silver nanowires suspension for the production of transparent and conductive  
544 electrodes by screen printing. *Applied Surface Science*, 394(Supplement C), 160–168.  
545 <https://doi.org/10.1016/j.apsusc.2016.10.073>
- 546 Hong, X., Wen, J., Xiong, X., & Hu, Y. (2016). Shape effect on the antibacterial activity of silver  
547 nanoparticles synthesized via a microwave-assisted method. *Environmental Science and Pollution  
548 Research*, 23(5), 4489–4497. <https://doi.org/10.1007/s11356-015-5668-z>
- 549 Ilić, V., Šaponjić, Z., Vodnik, V., Potkonjak, B., Jovančić, P., Nedeljković, J., & Radetić, M. (2009). The  
550 influence of silver content on antimicrobial activity and color of cotton fabrics functionalized with  
551 Ag nanoparticles. *Carbohydrate Polymers*, 78(3), 564–569.  
552 <https://doi.org/10.1016/j.carbpol.2009.05.015>
- 553 Kaur, R., & Liu, S. (2016). Antibacterial surface design – Contact kill. *Progress in Surface Science*, 91(3),  
554 136–153. <https://doi.org/10.1016/j.progsurf.2016.09.001>
- 555 Kipphan, H. (Ed.). (2001). *Handbook of Print Media: Technologies and Production Methods*. Springer-  
556 Verlag. <https://doi.org/10.1007/978-3-540-29900-4>
- 557 Korani, M., Ghazizadeh, E., Korani, S., Hami, Z., & Mohammadi-Bardbori, A. (2015). Effects of silver  
558 nanoparticles on human health. *European Journal of Nanomedicine*, 7(1), 51–62.  
559 <https://doi.org/10.1515/ejnm-2014-0032>
- 560 Kvítek, L., Panáček, A., Soukupová, J., Kolář, M., Večeřová, R., Pucek, R., Holecová, M., & Zbořil, R.  
561 (2008). Effect of Surfactants and Polymers on Stability and Antibacterial Activity of Silver  
562 Nanoparticles (NPs). *The Journal of Physical Chemistry C*, 112(15), 5825–5834.  
563 <https://doi.org/10.1021/jp711616v>
- 564 Lagaron, J. M., Catalá, R., & Gavara, R. (2004). Structural characteristics defining high barrier properties  
565 in polymeric materials. *Materials Science and Technology*, 20(1), 1–7.  
566 <https://doi.org/10.1179/026708304225010442>
- 567 Martins, N. C. T., Freire, C. S. R., Pinto, R. J. B., Fernandes, S. C. M., Neto, C. P., Silvestre, A. J. D.,  
568 Causio, J., Baldi, G., Sadocco, P., & Trindade, T. (2012). Electrostatic assembly of Ag  
569 nanoparticles onto nanofibrillated cellulose for antibacterial paper products. *Cellulose*, 19(4),  
570 1425–1436. <https://doi.org/10.1007/s10570-012-9713-5>
- 571 Morones, J. R., Elechiguerra, J. L., Camacho, A., Holt, K., Kouri, J. B., Ramírez, J. T., & Yacaman, M. J.  
572 (2005). The bactericidal effect of silver nanoparticles. *Nanotechnology*, 16(10), 2346.  
573 <https://doi.org/10.1088/0957-4484/16/10/059>
- 574 Nair, S. S., Zhu, J., Deng, Y., & Ragauskas, A. J. (2014). High performance green barriers based on  
575 nanocellulose. *Sustainable Chemical Processes*, 2, 23. <https://doi.org/10.1186/s40508-014-0023-0>
- 576 Pal, S., Tak, Y. K., & Song, J. M. (2007). Does the Antibacterial Activity of Silver Nanoparticles Depend  
577 on the Shape of the Nanoparticle? A Study of the Gram-Negative Bacterium Escherichia coli.  
578 *Applied and Environmental Microbiology*, 73(6), 1712–1720.  
579 <https://doi.org/10.1128/AEM.02218-06>

580 Rai, M. k., Deshmukh, S. d., Ingle, A. p., & Gade, A. k. (2012). Silver nanoparticles: the powerful  
581 nanoweapon against multidrug-resistant bacteria. *Journal of Applied Microbiology*, *112*(5), 841–  
582 852. <https://doi.org/10.1111/j.1365-2672.2012.05253.x>

583 Ramaraju, B., Imae, T., & Destaye, A. G. (2015). Ag nanoparticle-immobilized cellulose nanofibril films  
584 for environmental conservation. *Applied Catalysis A: General*, *492*(Supplement C), 184–189.  
585 <https://doi.org/10.1016/j.apcata.2014.12.045>

586 Rodionova, G., Saito, T., Lenes, M., Eriksen, Ø., Gregersen, Ø., Fukuzumi, H., & Isogai, A. (2012).  
587 Mechanical and oxygen barrier properties of films prepared from fibrillated dispersions of  
588 TEMPO-oxidized Norway spruce and Eucalyptus pulps. *Cellulose*, *19*(3), 705–711.  
589 <https://doi.org/10.1007/s10570-012-9664-x>

590 Schindelin, J., Arganda-Carreras, I., Frise, E., Kaynig, V., Longair, M., Pietzsch, T., Preibisch, S.,  
591 Rueden, C., Saalfeld, S., Schmid, B., Tinevez, J.-Y., White, D. J., Hartenstein, V., Eliceiri, K.,  
592 Tomancak, P., & Cardona, A. (2012). Fiji: an open-source platform for biological-image analysis.  
593 *Nature Methods*, *9*(7), 676–682. <https://doi.org/10.1038/nmeth.2019>

594 Schneider, C. A., Rasband, W. S., & Eliceiri, K. W. (2012). NIH Image to ImageJ: 25 years of image  
595 analysis. *Nature Methods*, *9*(7), 671–675. <https://doi.org/10.1038/nmeth.2089>

596 Slavin, Y. N., Asnis, J., Häfeli, U. O., & Bach, H. (2017). Metal nanoparticles: understanding the  
597 mechanisms behind antibacterial activity. *Journal of Nanobiotechnology*, *15*(1), 65.  
598 <https://doi.org/10.1186/s12951-017-0308-z>

599 Smetana, A. B., Klabunde, K. J., Marchin, G. R., & Sorensen, C. M. (2008). Biocidal Activity of  
600 Nanocrystalline Silver Powders and Particles. *Langmuir*, *24*(14), 7457–7464.  
601 <https://doi.org/10.1021/la800091y>

602 Sofi, S. A., Singh, J., Rafiq, S., Ashraf, U., Dar, B. N., & Nayik, G. A. (2018). A Comprehensive Review  
603 on Antimicrobial Packaging and its Use in Food Packaging. *Current Nutrition & Food Science*,  
604 *14*(4), 305–312. <https://doi.org/10.2174/1573401313666170609095732>

605 Syverud, K., & Stenius, P. (2008). Strength and barrier properties of MFC films. *Cellulose*, *16*(1), 75.  
606 <https://doi.org/10.1007/s10570-008-9244-2>

607 TAPPI Standard. (2009). *T 448 om-09 - Water vapor transmission rate of paper and paperboard at 23°C*  
608 *and 50% RH*. Technical Association of the Pulp and Paper Industry, New York.

609 Turbak, A. F., Snyder, F. W., & Sandberg, K. R. (1983). Microfibrillated Cellulose, a New Cellulose  
610 Product: Properties, Uses, and Commercial Potential. *J. Appl. Polym. Sci.: Appl. Polym. Symp.*;  
611 *(United States)*, *37*. <https://www.osti.gov/scitech/biblio/5062478>

612 Uddin, K. M. A., Orelma, H., Mohammadi, P., Borghei, M., Laine, J., Linder, M., & Rojas, O. J. (2017).  
613 Retention of lysozyme activity by physical immobilization in nanocellulose aerogels and  
614 antibacterial effects. *Cellulose*, *24*(7), 2837–2848. <https://doi.org/10.1007/s10570-017-1311-0>

615 Vak, D., Weerasinghe, H., Ramamurthy, J., Subbiah, J., Brown, M., & Jones, D. J. (2016). Reverse  
616 gravure coating for roll-to-roll production of organic photovoltaics. *Solar Energy Materials and*  
617 *Solar Cells*, *149*, 154–161. <https://doi.org/10.1016/j.solmat.2016.01.015>

618 Vartiainen, J., Laine, C., Willberg-Keyriläinen, P., Pitkänen, M., & Ohra-aho, T. (2017). Biobased  
619 mineral-oil barrier-coated food-packaging films. *Journal of Applied Polymer Science*, *134*(9).  
620 <https://doi.org/10.1002/app.44586>

621 Visnapuu, M., Joost, U., Juganson, K., Künnis-Beres, K., Kahru, A., Kisand, V., & Ivask, A. (2013).  
622 Dissolution of Silver Nanowires and Nanospheres Dictates Their Toxicity to Escherichia coli.  
623 *BioMed Research International*, *2013*, 1–9. <https://doi.org/10.1155/2013/819252>

- 624 Wu, B., Geng, B., Chen, Y., Liu, H., Li, G., & Wu, Q. (2017). Preparation and characteristics of TEMPO-  
625 oxidized cellulose nanofibrils from bamboo pulp and their oxygen-barrier application in PLA  
626 films. *Frontiers of Chemical Science and Engineering*, *11*(4), 554–563.  
627 <https://doi.org/10.1007/s11705-017-1673-8>
- 628 Xu, Y., Li, S., Yue, X., & Lu, W. (2017). Review of Silver Nanoparticles (AgNPs)-Cellulose Antibacterial  
629 Composites. *BioResources*, *13*(1), 2150-2170–2170. <https://doi.org/10.15376/biores.13.1.Xu>
- 630 Yildirim, S., Röcker, B., Pettersen, M. K., Nilsen-Nygaard, J., Ayhan, Z., Rutkaite, R., Radusin, T.,  
631 Suminska, P., Marcos, B., & Coma, V. (2018). Active Packaging Applications for Food.  
632 *Comprehensive Reviews in Food Science and Food Safety*, *17*(1), 165–199.  
633 <https://doi.org/10.1111/1541-4337.12322>
- 634 Yu, Z., Wang, W., Kong, F., Lin, M., & Mustapha, A. (2019). Cellulose nanofibril/silver nanoparticle  
635 composite as an active food packaging system and its toxicity to human colon cells. *International*  
636 *Journal of Biological Macromolecules*, *129*, 887–894.  
637 <https://doi.org/10.1016/j.ijbiomac.2019.02.084>